Nature Communications

https://doi.org/10.1038/s41467-026-71314-1

Article in Press

Differential cellulose distribution drives polarized growth of cotton fibers

Received: 15 July 2025

Accepted: 19 March 2026

Cite this article as: Wang, G., Wang, J., Yang, H. *et al.* Differential cellulose distribution drives polarized growth of cotton fibers. *Nat Commun* (2026). https://doi.org/10.1038/s41467-026-71314-1

Guangda Wang, Jie Wang, Huanhuan Yang, Jingxia Wu, Yanjun Yu, Xiaxia Zhang, Juan Tian, Yinping Ma, Gui-xian Xia, Yongbiao Xue, Staffan Persson, Lvwen Zhou & Zhaosheng Kong

Differential Cellulose Distribution Drives Polarized Growth of Cotton Fibers

Guangda Wang[1], Jie Wang[2], Huanhuan Yang[1,3], Jingxia Wu[1,3], Yanjun Yu[1], Xiaxia Zhang[1], Juan Tian[1], Yinping Ma[1], Gui-xian Xia[1], Yongbiao Xue[3,4], Staffan Persson[5,6], Lvwen Zhou[7*] and Zhaosheng Kong[1,2,3*]

[1]State Key Laboratory of Microbial Diversity and Innovative Utilization, Institute of Microbiology, Chinese Academy of Sciences, Beijing 100101, China

[2]Houji Laboratory in Shanxi Province, Shanxi Agricultural University, Taigu 030801, China

[3]University of Chinese Academy of Sciences, Beijing 100049, China

[4]State Key Laboratory of Plant Cell and Chromosome Engineering, Institute of Genetics and Developmental Biology, Chinese Academy of Sciences, Beijing 100101, China

[5]Department of Plant & Environmental Sciences, Copenhagen Plant Science Center, University of Copenhagen, 1871 Frederiksberg, Denmark

[6]Joint International Research Laboratory of Metabolic and Developmental Sciences, School of Life Sciences and Biotechnology, Shanghai Jiao Tong University, Shanghai 200240, China

[7] Zhejiang-Italy Joint Lab for Smart Materials and Advanced Structures, Faculty of Mechanical Engineering & Mechanics, Ningbo University, Ningbo 315211, China

[*]Correspondence should be addressed to

Lvwen Zhou, Email: zhoulvwen@nbu.edu.cn

Zhaosheng Kong, Email: zskong@im.ac.cn

Zhaosheng Kong, http://orcid.org/0000-0003-3788-7883

Abstract

Plant cell morphogenesis relies on the mechanical properties of the primary cell wall, yet it remains unclear which components predominantly regulate wall extensibility. Cotton fibers, highly elongated single cells, offer a unique system to investigate polarized cell expansion. Here, by combining atomic force microscopy and cellulose labeling, we find a basipetal gradient of cellulose microfibril density from the apex to the shank that underlies cell wall heterogeneity and directed cotton fiber elongation. Live-cell imaging shows that cellulose synthase complexes accumulate more densely toward the shank which is guided by specific microtubule organization and is supported by genetic disruption and microtubule perturbation. A mechanical model further demonstrates that a cellulose gradient is sufficient to reshape axial strain for directional growth. Collectively, our findings provide single-cell evidence for a cellulose-dependent mechanism of directional growth, expanding our understanding of primary cell wall extensibility in plant morphogenesis and offering potential strategies to improve cotton fiber quality.

Introduction

Plant primary cell walls (PCWs), mainly composed of three distinct polysaccharides (cellulose, hemicelluloses and pectins), are strong but extensible extracellular structures that critically underpin cell growth and environmental adaptation [1,2]. From a biomechanical perspective, plant cell expansion is driven by the prevalent turgor pressure within the cells. And the heterogeneity of plant cell walls, including the spatial distribution of cell wall components and their structural organizations, results in anisotropic mechanical responses to turgor pressure. Such behavior would convert the isotropic internal pressure into directionally biased deformation, contributing to the formation of diverse cell shapes. Therefore, the mechanical properties that determine dynamic extensibility of PCW are central to plant cell growth and morphogenesis [3,4]. However, how different cell wall components determine anisotropic expansion of plant cells remain controversial. Homogalacturonans (HGs), the most abundant form of pectins, are often considered as major determinants of plant cell wall heterogeneity [5-7]. However, new computational models support a prominent role of sliding cellulose microfibrils in cell wall extensibility during constant stress [3]. Due to substantial differences in cell types and contexts that these observations have been made, we argue that a single-cell system that combines diffuse and tip-related growth might be ideal to address cell wall organization and the driving force for plant cell growth.

Cotton fibers are highly elongated and unbranched single cells differentiated from the

ovule epidermis, and are one of the longest plant cells characterized [8]. Elongating fiber cell walls typically contain 40% cellulose, 25-30% hemicelluloses, 30-35% pectins, and a variety of wall proteins [9]. Notably, the length of cotton fibers can reach 3-6 cm, which is 1000-3000 times greater than the diameter during the elongating stage [10]. After the PCW-dominated rapid elongation stage, cotton fibers gradually stop elongating and enter a secondary cell wall thickening stage. In this phase, cellulose accumulates to become the most prevalent wall components, accounting for > 95% dry weight of cotton fibers [11]. Owing to the highly polarized unicellular feature and abundant cellulose content, cotton fibers have long been regarded as an excellent model for investigating plant cell elongation and cellulose biosynthesis [12]. Elongating cotton fiber cells may therefore be a suitable single-cell system to decipher how different cell wall components contribute to heterogenous wall organization and dynamic extensibility during plant cell growth [9].

Qin and Zhu proposed a linear growth mode of cotton fibers that combines tip and diffuse growth, based on cytoskeletal organization using immunostaining [13]. Ten years later, our previous studies provided the first live-cell observations on the cytoskeletal organization in elongating fiber cells, and further proposed a unique, tip-biased diffuse growth mode for cotton fibers [14,15]. However, direct exploration of wall structures and mechanics that drive cotton fiber elongation is still lacking. Here, using atomic force microscopy (AFM) alongside cellulose labeling, we show that differential cellulose deposition underpins the mechanical properties of cotton fiber cell walls. By integrating

live-cell imaging with computational modeling, we propose that a basipetal cellulose gradient, tightly associated with the microtubule-mediated spatial distribution of cellulose synthase complexes (CSCs), drives cotton fiber elongation. This unique cellulose deposition pattern not only supports tip-biased diffuse growth in cotton fibers but further highlights the indispensable role of cellulose in regulating plant cell expansion at the single-cell level.

Results

Cotton fiber cell walls are soft at the tip, with stiff shanks

After anthesis, cotton fibers initiate and proceed into a rapid elongating stage (Fig.1a). This stage relies on the heterogeneous extensibility of the PCWs. To assess mechanical characteristics, as well as morphological surface differences along the PCWs, we examined the apparent elastic modulus and apparent stiffness via AFM scanning (Fig. 1b and c). Cell wall elastic modulus describes the intrinsic elasticity of the cell wall material, while cell wall stiffness reflects the overall resistance of the wall to deformation under an applied force. In our AFM measurements, the reported modulus is best interpreted as an apparent elastic modulus, as the fiber walls show adhesion and nonlinear force-displacement behavior. Although AFM indentation primarily measures the mechanical response perpendicular to the cell wall surface, it provides valuable insight into the local mechanical properties that may influence wall extensibility and morphogenesis in growing tissues [16-19]. Therefore, in this study AFM-derived apparent modulus and stiffness are

used here as comparative indicators of the local mechanical state, which could be interpreted as a relative mechanical landscape and is informative for understanding cotton fiber elongation. We found a gradual increase in apparent modulus of cotton fiber cell walls at 7 DPA (corresponding to rapid elongation) as compared to 3 DPA (early elongating stages/late initiating stage), which may underlie an enhanced capacity to bear turgor-generated stress during fiber expansion (Fig. 1c and Supplementary Fig.1). By comparing AFM-derived mechanical parameters across two major cotton cultivars, i.e. the upland cotton (*Gossypium* hirsutum) TM-1 and the sea-island cotton (*Gossypium* barbadense) Hai7124 harboring longer fibers, we found that Hai7124 exhibited lower apparent elastic modulus and stiffness than TM-1 (Fig. 1c). This association between a more mechanically compliant primary wall and greater final fiber length suggests a possible link between early wall mechanics and fiber elongation capacity. If confirmed in broader cotton populations, such features could potentially serve as mechanical indicator for fiber-quality breeding.

We next analyzed mechanical properties at different regions of individual fiber cells. Strikingly, the cell walls near the tip exhibited lower apparent modulus and stiffness, suggesting that the PCWs of cotton fibers are softer and mechanically more compliant at the tip that we interpret as conferring a higher local expansion potential (Fig. 1d), most likely related to fiber tip-biased diffuse growth mode. To further test whether this mechanical heterogeneity correlates with regional differences in wall deformation, we performed osmotic shrinkage assays. Treatment of 3 DPA fibers with 0.8 M mannitol

caused a significantly larger reduction in width at the tip than at the shank, whereas fibers under water conditions showed minimal changes (Fig. 1e and f). These results indicate that apical walls are more deformable under turgor-related perturbation, in agreement with their lower apparent stiffness and modulus.

To further confirm the tip-biased elongation of fiber cells, we attempted to visualize newly forming cell walls in cotton fibers from the cultured ovules via a click-chemistry-based strategy [20]. We used a glucose that contains a clickable group (2-Azido-2-deoxy-D-glucose, aGlu), which was applied in the growth medium. This molecule was readily incorporated into the fiber cell walls (Fig. 2a and b), thus reflecting newly formed cell walls that we could track by a click reaction to the dibenzocyclooctyl-linked cyanin 5 (DBCO-Cy5) (Supplementary Fig. 2a-c). While we are unsure what cell wall polymer that is labelled by this approach, we could therefore monitor the incorporation of glucose into the extracellular matrix (Supplementary Fig. 2d). These analyses confirmed a tip-biased growth pattern of cotton fibers (Fig. 2c and Supplementary Fig. 2a-c).

A gradient of cellulose accumulation determines heterogeneous cell wall properties of cotton fibers

Local modifications of pectins play a crucial role in cell wall extensibility [6,7,21,22]. To see whether the ratio of de-methyl- / methyl-esterification of pectins in cotton fibers could explain the cell wall heterogeneity we observed in our AFM assays, we performed immunolabelling assays with two monoclonal antibodies, JIM5 and JIM7, that specifically

recognize the lowly-esterified HGs (JIM5) and highly methyl-esterified HGs (JIM7), respectively [21]. Notably, both JIM5- and JIM7-labeling were uniformly distributed along cotton fibers (Supplementary Fig. 3a and b). To further investigate the role of pectins in fiber extension, we treated the fibers with the pectinase. However, no obvious impact was detected on cotton fiber growth and development (Supplementary Fig. 3c). We therefore inferred that pectin modifications if involved, are unlikely to have major effects on cotton fiber development or on the heterogeneous cell wall formation that we observed.

Cellulose is the principal load-bearing cell wall component, and we therefore speculated that differential distribution of cellulose may contribute to the heterogeneity of cotton fiber PCWs [9,23]. To test this hypothesis, we assessed the thickness of cellulosic cell walls of cotton fibers between the apex and shanks and performed functional perturbations. Here, we used calcofluor-white (CFW) that preferentially binds cellulose in cell walls of land plants and quantified the full width at half maximum (FWHM) of the cross-sectional CFW intensity profile as an indicator of the apparent width of cellulosic PCWs (Fig. 3a and b). These results revealed a clear difference of CFW-derived signal width between fiber shank and apex, indicating higher cellulose accumulation in the shank than in the apex. In parallel, staining with the cellulose-specific dye S4B, we found transverse banded labeling patterns that are in line with previous observation of cellulose microfibrils by transmission electron microscopy[24], and likewise showed stronger cellulose accumulation in the fiber shanks (Fig. 3c and d). Interestingly, we also found that within apex cross-sections, the CFW-derived apparent wall signal width positively

correlated with fiber diameter (Fig. 3e). Together with the differential cellulose accumulation between fiber shank and apex, these data infer a progressive increase in cellulose deposition along the fiber axis, which may contribute to heterogeneous wall mechanics and underpin anisotropic expansion of the fibers. To functionally test whether cellulose deposition is required for fiber growth and cell wall heterogeneity, we used either the cellulose biosynthesis inhibitor (CBI) isoxaben[25] or cellulase R-10 to reduce cellulose deposition in the fibers at 2 DPA. Both treatments led to loss of the anisotropic growth behavior of the cotton fibers, indicating that cellulose deposition is indispensable for cotton fiber development (Supplementary Fig. 4). Taken together, these results support differential cellulose deposition along the fiber axis, which is consistent with and may contribute to the observed cell wall heterogeneity and directed cotton fiber elongation.

The CMF deposition gradient is associated with differential CSC distribution across the cotton fiber surface

PCW cellulose is presumed to be synthesized by GhCESA1, GhCESA3 and GhCESA6 in cotton fiber cells [26,27]. To directly observe the cellulose biosynthesis and the deposition of CMFs in elongating cotton fibers, we generated mNeoGreen-tagged GhCESA3 single, or mNeoGreen-CESA3 and mCherry-TUB9 dual, fluorescent markers that label CSCs and microtubules, respectively. Using these lines, we performed live-cell imaging to track the spatial distribution and dynamics of CSCs. As shown in Supplementary Fig. 5, we observed PM-localized mNeoGreen-CESA3 particles in various cell types, such as pavement and petiole cells. These particles moved along linear trajectories, similar to

what has been reported in Arabidopsis, with movement that coincided with underlying MTs (Fig. 4a). In addition, we also observed CESA3 fluorescence from cytoplasmic foci that moved erratically, and likely resemble that of small CSC compartments (SmaCCs) or MT-associated CESA compartments (MASCs) that have been reported on in Arabidopsis [28,29].

To further explore the CSC dynamics in elongating cotton fibers, we imaged both initiating and elongating fibers. Similar to other cell types, fluorescent CESA3 particles localized to the PM in fiber cells across these developmental stages (Fig. 4b and Supplementary Fig. 5a-d). The speed of the PM-located CSCs is thought to correspond to the catalytic activity of the CSCs [29]. Therefore, we quantified the speed of the PM-localized CSCs across various cotton cell types. Surprisingly, while the CSC moved with about 150 nm/min in pavement (mean ± SD = 148.3 ± 63.6, five cells) and petiole cells (mean ± SD = 147.1 ± 68.6, five cells), the CSCs moved significantly faster in the two developmental stages (initiation, mean ± SD = 224.5 ± 84.2, five cells; elongation, mean ± SD = 365.2 ± 110.4, five cells) of cotton fibers (Fig. 4c and d). Taken together, these data indicate a higher catalytic activity of CSCs in cotton fiber cells than in pavement cells or petiole cells, likely due to high demands of cellulose in the rapidly expanding fiber cells.

As the shanks and the apex regions of cotton fiber cells exhibit heterogeneous cell wall mechanics and differences in cellulose levels, we speculated that the catalytic activity of CSCs might vary correspondingly. To test this, we imaged mNeoGreen-CESA3 at the different regions of elongating fibers. However, only mild changes in CSC speed at the

different regions were detected (Fig. 4e and f, and Supplementary Movie 1). Alternatively, the density of PM-localized mNeoGreen-CESA3 particles appeared to be higher in fiber shanks than at the apex (Fig. 4e and g, Supplementary Fig 5e, and Supplementary Movie 2). We confirmed this observation by quantifying the number of fluorescent CSCs per area unit, where shanks had 0.84 CSCs per μm^2 and apex had only 0.59 CSCs per μm^2. Therefore, the increase in cellulosic PCWs along the cotton fiber is likely driven by a biased PM-localized CSC distribution.

The microtubule arrangement defines the differential CSC distribution for cotton fiber elongation

CSCs typically track along MTs, which may define CSC trajectories in plant cells [29,30]. To corroborate that such relationship also determines the spatial patterning of CSCs in cotton fibers, we examined the cortical MT organization in cotton fiber cells at both the initiation and the elongation stages (Fig 5a, Supplementary Fig. 5f, and Supplementary Movie 3, 4). We observed a mesh-like MT array in fibers at the initiation stage. By contrast, the MT array was well-aligned and arranged perpendicular to the growth axis of elongating fiber cells. Correspondingly, we observed fluorescent CSCs moving along the MTs, with trajectories aligning with the MTs (Fig. 4c). We next assessed the MT organization in the shanks and the apex regions of elongating cotton fiber cells. As expected, we observed reduced MT density at the apex as compared to the shanks, which corresponded well with the observed CSC distribution (Fig. 5a-c). Additionally, we detected a MT depleted

zone (MDZ) in the fiber cell apex, similar to our previous observations in cotton fibers and in Arabidopsis trichomes [14,31]. Then, we further validated the functional relationship between MTs and CSCs by pharmacological treatments in cotton fiber cells. Here, the MT stabilizing drug Taxol or MT nucleation inhibiting drug Propyzamide reduced the differences in MT density between the shanks and the apex of fiber cells (Fig. 5d and e). Surprisingly, these treatments led to an even distribution of CSCs across the fiber cell PM (Supplementary Fig. 5g and h). These fibers did not display tip-biased fiber elongation as illustrated by the chase-labelling experiments (Fig. 5f).

The CSCs are guided by MTs via the protein CSI1 in Arabidopsis [30,32]. Thus, we first validated the biochemical interaction between GhCSI1 and GhCESA3 (Supplementary Fig. 6a and b). To further explore the relationship of CSC and MTs in cotton, we used the CRISPR-Cas9 technology to mutate the *GhCSI1* paralogs (*Gh_A11G212800, Gh_D11G239500*) (Supplementary Fig. 6c), which are predominantly expressed in development fiber cells, of both the *At* and *Dt* cotton subgenomes as reported in CottonGVD database (https://db.cngb.org/cottonGVD/). Using advanced fiber information system (AFIS) measurements of cotton fiber lengths, we found that the CSI1-mutated lines had significantly shorter fibers compared to wild type (Supplementary Fig. 6d-f). These results indicate an important role of MT-guided CSC distribution to control tip-biased growth of cotton fibers.

Computational simulation of how CMF deposition patterns underpin cotton fiber

growth

To explore how CMFs support both directional expansion and differential growth of cotton fibers, we performed computational simulations. Some of the key modeling parameters are referenced from a previously reported cotton fiber model [33] (see also Supplementary Note 1). In our model the cell wall matrix and embedded CMFs are simplified to longitudinally arranged matrix spring segments and numerous transversely arranged CMF springs (Supplementary Fig. 7a), similar to what we observed with the S4B staining. This method allowed us to simulate and analyze the effects of different CMF deposition patterns on the polarized elongation of cotton fiber cells. According to our simulations, the uniformly distributed CMF springs along the cells led to equivalent strains along cell walls, which correlated with a diffuse expansion mode of plant cells (Supplementary Fig. 7b and c). By contrast, a gradient of CMF springs led to a gradually increasing strain at the apex (Fig. 5g and h, and Supplementary Movie 5), which is in line with our observations in cotton fiber cells.

Additionally, we noticed that the growth rate of the apex would reach saturation with the increase in shank-to-apex CMF density ratio in the model (Supplementary Fig. 7d). Similarly, at higher shank-to-apex CMF density ratios (e.g., greater than 6), the reduction in applied force will be less pronounced. (Supplementary Fig. 7e). These results indicated that maintaining a range of shank-to-apex CMF density ratio (i.e. 2 to 6) is sufficient to generate tip-biased cotton fiber elongation. Excessive CMF deposition differences between cotton fiber apexes and shanks would perhaps not be an efficient way to drive

cell expansion as this may lead to unnecessary amounts of cellulose at the shank. Our modelling data thus supports our live-cell imaging, where we observed a two-fold shank-to-apex ratio of CMF density. Collectively, our simulation results, together with the observed cellulose and mechanical heterogeneity, are consistent with a tip-biased diffuse growth mode of cotton fibers, in which apical regions exhibit higher elongation potential than the shank (Fig. 5i). In this model, elongation remains distributed along the fiber but is biased towards the apex.

Discussion

In this study, we provide insights into the cellular mechanisms underlying polarized growth in cotton fibers by revealing how differential cellulose deposition generates cell wall mechanical heterogeneity. In cotton fibers, our findings refine and extend the conventional view, largely derived from other plant systems, that cell wall extensibility is primarily regulated by pectin modifications, by highlighting a key contribution of cellulose-based reinforcement to wall mechanics and directional expansion in cotton fibers. Together, these results offer a mechanistic framework for understanding how cellulose-mediated wall heterogeneity supports polarized cell growth.

The hypothesis of microtubule-CMF co-alignment was proposed as early as the 1960s. However, until nearly half a century later, live-cell imaging of PCW CSCs was first

achieved in Arabidopsis hypocotyls [34]. And ten years later, CSCs involved in secondary wall synthesis were visualized using an inducible vascular system in Arabidopsis cell culture [35]. Cotton fiber cells, considered an ideal single-cell model for studying polarized cell elongation and cellulose synthesis, have long posed a challenge for live-cell imaging of CSC dynamics. These challenges have largely been due to the lack of suitable fluorescent tags and imaging techniques for intertwined fiber cells that are embedded in the cotton ovules. We overcame these challenges and managed to track CSC dynamics and microtubule organization in live cotton fiber cells. Notably, CSCs moved faster in cotton fibers than in other cell types, indicating increased catalytic activity of the CSCs presumably to maintain adequate cellulose synthesis to support the growth of the fibers. These results are somewhat similar to those observed in Arabidopsis during the transition between PCW to SCW synthesis where SCW CSCs moved twice as fast as the PCW CSCs [36]. This led the authors in the study to speculate that the cellulose demand during SCW was simply driving the change in catalytic rate, which perhaps is due to post-translational modifications on CSC proteins that could regulate the speed [37]. We assume that certain post-translational modifications may also drive the changes in speed in cotton.

Interestingly, we detected a differential distribution of CSCs in fiber cells, with a gradual increase in CSC density along the shank, coinciding with a gradient of cellulose deposition and spatial differences in wall deformation potential as inferred from AFM measurements and osmotic assays. Notably, this basipetal differential CSC distribution coincided with, and depended on, a gradually denser MT array. It is plausible that this

distinct MT organization could reflect cell wall strains during development, in light of recent evidence that cortical microtubules can respond to mechanical cues in plants [29,38]. However, detailed mechanism remains to be specifically tested in cotton fiber cells. It is also plausible that the uneven basipetal distribution of “polarity” proteins that regulate MT nucleation and stability may be involved in maintaining this organization [4,39]. Interestingly, both our previous work and studies by other groups have identified a microtubule-depleted zone (MDZ) at the fiber apex [14,31,40,41]. We speculate that this MDZ, together with the transverse MT arrays exhibiting basipetal gradient accumulation, forms a specific MT architecture that regulates the anisotropic elongation of cotton fibers. However, the molecular and mechanical basis underlying MDZ formation and its role in shaping the fiber tip morphology remain intriguing questions for future exploration. The detailed establishment of tip shape is likely to involve additional biochemical and biomechanical mechanisms. Spatial organization of the cytoskeleton and wall-modifying or structural proteins is expected to fine-tune apex morphology, potentially through mechanisms that are not solely determined by turgor-driven wall expansion. Dissecting these processes will require future targeted studies.

Heterogeneous extensibility of PCWs is essential to plant cell morphology as it regulates the direction of plant cell expansion [42,43]. Previous studies highlighted pectin modifications as key factors in regulating cell wall extensibility. The abundant type of pectins in PCWs, the homogalacturonans (HGs), are synthesized in a methylesterified form and undergo a de-methylesterification process after insertion into the cell walls [6].

The de-methylesterified HGs can either reduce cell wall stiffness to promote the longitudinal elongation of hypocotyl cells [44,45] or strengthen the wall mechanically by crosslinking with calcium, as seen in pollen tube shanks during tip growth [21]. Moreover, the HGs can also form nanofilaments to mediate asymmetric cell wall expansion and lobe formation in pavement cells [46]. However, our immunolabeling and enzymatic results suggest that pectins have little effect on cotton fiber elongation, which is also consistent with some previous enzymatic studies [47]. On the other hand, the pectin abundance reported in prior studies (typically after 5 DPA) [9] likely reflects its increasing role in the formation of the cotton fiber middle lamella (CFML) and in mediating inter-fiber adhesion and tissue-level coordination [48], rather than directly controlling polarized single-cell elongation. This view is further supported by temporal gene expression data, which show upregulation of pectin-modifying enzymes primarily at later developmental stages [49-51]. And some fiber-specific PME genes were expressed predominantly at the secondary wall thickening stage [52]. Similarly, experimental manipulation of hemicellulose levels has not been shown to significantly alter fiber elongation during early growth [49]. Thus, in our system, cellulose emerges as a major mechanical contributor to fiber extensibility during the early elongation stage, whereas pectins and hemicelluloses are more likely to participate in the subsequent remodeling and coordination of fiber cell wall architecture at later developmental stages. In addition, it is possible that gradients in biochemical wall loosening factors, such as expansins or XTHs, may collaborate with cellulose to facilitate cotton fiber growth by modulating cell wall mechanical properties. Future studies focused

revealing the spatial distribution of wall loosening factors in cotton fibers would provide valuable insights on the role of plant cell wall mechanical regulation during growth.

Importantly, our findings uncovered that a gradual increase in cellulose deposition regulated the cell wall tip-biased extensibility, which is consistent with the recently proposed CMF sliding model [3]. In this model, deposition of CMFs determines the orientation of plant cell expansion by providing anisotropic resistance to internal turgor pressure. When extended to the tissue level, this model suggests that thickened outer walls of cylindrical tissues generate additional tissue tension [4]. Supporting this mechanical model, recent studies have revealed the existence of tissue stress that is functional in driving coordinated growth between cell layers in the tissues [53,54]. In our computational modeling, pectin and hemicellulose were simplified as isotropic matrix components, consistent with their reported homogeneous distribution during early fiber elongation. While this approach highlights the dominant mechanical role of cellulose gradients, we acknowledge that future models could benefit from integrating more detailed spatial and biochemical properties of matrix polysaccharides to better capture the complexity of fiber cell wall mechanics. It is worth noting that the fiber elongation was only considered at the longitudinal dimension under various CMF deposition patterns in our simulations for simplification. Rather than acting as the determinant of whole fiber cell morphogenesis, in our study the CMF deposition is therefore best viewed as a key contributor to polarized growth. Indeed, gradient cellulose deposition confers unique

mechanical properties to the cotton fiber cell wall, enabling greater extensibility in the apex regions. These mechanical properties support the tip-biased diffuse growth mode we previously proposed [14]. Consistent with this view, our mechanical modelling predicts a gradual decrease in axial strain rate from the apex toward the shank. As high-resolution tracking of local fiber elongation remains technically challenging, our current data only support a tip-biased diffuse growth mode rather than a fully resolved growth gradient. Future development of more stable fiducial labeling and dedicated imaging or microfluidic platforms will be important to directly measure local growth rates and further refine the growth model of cotton fibers. In addition, a more complete quantification of how transverse cellulose reinforcement contributes to effective longitudinal stiffness will require future in-plane mechanical measurements and high-resolution strain mapping in both circumferential and axial directions.

Taken together, our work advances the emerging paradigm that cellulose gradients are critical for plant cell morphogenesis. By providing single-cell level evidence for a cellulose microfibril-dependent expansion mechanism, this study also highlights how targeted manipulation of cellulose distribution may improve fiber qualities. Future investigations focusing on modulating the expression or localization of cellulose synthase regulators can enable targeted manipulation of wall mechanics in specific fiber zones, which could offer new insights into cotton fiber quality improvement.

Methods

Plant materials and growth conditions

The cotton cultivars TM-1 and Hai7124 were used as the wild type control for the upland cotton (Gossypium hirsutum) and the sea-island cotton (Gossypium barbadense), respectively. The TM-1 was also used as recipient of the proCESA3-mNeoGreen-CESA3 and the proCESA3-mNeoGreen-CESA3-proTUB1-mCherry-TUB9 constructs. Cotton transformation was performed as described previously [14]. All the cotton lines were grown in the field under normal farming practices, or in a greenhouse with long-day (16 h light/8 h dark) conditions at 28 ℃. Flowers were tagged on the day of anthesis, and fibers were dissected from ovules in bolls at various DPA for further analyses. Bolls from similar positions (primarily the middle boll positions) were uniformly harvested for fiber analyses.

Plasmids Construction

The constructs of proCESA3-mNeoGreen-CESA3 and proCESA3-mNeoGreen-CESA3-proTUB1-mCherry-TUB9 were generated to obtain stable transgenic cotton lines expressing the fluorescent marker of the mNeoGreen-tagged CESA3, or cotton lines simultaneously expressing the double fluorescent marks of mNeoGreenCESA3 and mCherry-TUB9. The Phanta DNA polymerase with high fidelity (Vazyme Biotech Co., Ltd, AWS1207) was used to amplify all the required gene products as described in the

previous studies [55,56]. In detail, for the construct of proCESA3-mNeoGreen-CESA3, the promoter (1,930 bp upstream from the initiation ATG) of CESA3 gene (Gh_A08G167200), the coding sequence of CESA3 genes and the 1,125 bp downstream untranslated region was amplified from the genomic DNA, respectively. And these fragments fused with the fragment of mNeoGreen were used to obtain the final expression constructs through the in-fusion cloning using the DNA Assembly Mix PLUS KIT (LABLEAD, D0204P). For the construct of proCESA3-mNeoGreen-CESA3-proTUB1-mCherry-TUB9, the promoter (1,608 bp upstream from the initiation ATG) of TUB1 gene (Gh_A08G207900), the coding sequence of TUB9 gene (Gh_A08G206600) and the 931bp downstream untranslated region was amplified from the genomic DNA, respectively. These fragments fused with the DNA fragment encoding mCherry were insert to the construct of proCESA3-mNeoGreen-CESA3 through the in-fusion cloning using the DNA Assembly Mix PLUS KIT (LABLEAD, D0204P) to obtain the final expression construct.

Atomic Force Microscopy

Ovules at different developmental stages were collected, and fiber bundles were gently cut from the ovules and mounted on clean glass slides, then allowed to air-dry at room temperature. Atomic force microscopy (AFM) imaging and nano-indentation were performed using a Dimension Icon AFM (Bruker, Santa Barbara, CA, USA) operating in PeakForce Tapping mode with ScanAsyst and Quantitative Nanomechanical Property Mapping (QNM) as described previously [57]. All images were acquired at 512 × 512 pixels over 2 μm × 2 μm scan areas positioned on visually flat regions of the fiber surface near

the tip or the shank.

ScanAsyst-Air silicon-nitride probes (Bruker; nominal spring constant 0.2-0.7 N/m; tip radius ~10 nm) were used. The actual spring constant was calibrated by the thermal-tune method and the deflection sensitivity was determined on a hard glass surface using the NanoScope software. During PeakForce imaging, the force setpoint was adjusted to keep the maximum load below ~5 nN, which resulted in an indentation depths on the range of ~100 nm. At every pixel a force curve was recorded and later analyzed in NanoScope Analysis 1.8 (Bruker). Regions of interest selected on relatively smooth areas of the fiber surface were used for statistical analysis. Modulus and stiffness are derived from force maps, with a built-in Hertz contact model with adhesion enabled, as implemented in the software. Because the fiber cell walls exhibited pronounced adhesive minima and nonlinear force-displacement behavior, the AFM-derived moduli should be regarded as apparent elastic modulus. Pixels affected by edges, dust, obvious baseline drift or poor fits were excluded from the analysis.

Ovule culture in vitro culture and chase-labelling of newly formed cell walls

The fresh flowers at 2 DPA were harvested from the cotton plants. The ovaries were then sterilized with 70% ethanol after removing petals and the sepals. The cotton ovules (2 DPA) were disserted from the bolls and cultured at 28 °C in BT medium in dark. To access the influence of cellulose for cotton fiber development and morphology, either 0.1 μM of Isoxaben (DR. EHRENSTORFER, DRE-C14480000) or the 0.1% (w/v) of cellulase R-10 (Yakult, L0112) was applied into the medium. The growth of cultured cotton fibers were

observed either by a stereoscope or by a confocal microscope.

To determine the newly formed cell walls in cultured cotton fibers, 2.5 μM of 2-Azido-2-deoxy-D-glucose (aGlu; HARVEYBIO, A33673) were applied or washed out to the medium in two stages of 4-hour periods. The ovules were washed three times with PBS (pH=7.4) and then labelled with 1 μM DBCO-Cy5 (AAT Bioquest, Lot: 923) for 20 min. Fluorescence of labeled cotton fibers was visualized via a confocal microscope (Leica SP8, excited at 633 nm, EM 650–670 nm) under a 40X objective.

Immunolabelling of pectins in cotton fiber cells

The cotton ovules were harvested from fresh flowers at 2-3 DPA and then fixed for 30 min with 4% (w/v) paraformaldehyde in PBS buffer (pH=7). After three times washes with PBS, the ovules were then incubated with 3% (w/v) milk protein in PBS buffer to block non-specific binding sites. The primary antibodies (JIM5 or JIM7; PlantProbe) were diluted in 1:10 with PBS and incubated with the ovules overnight at 4 ℃. After three washes with PBS, the ovules were then incubated with the secondary antibody (FITC conjugated goat anti-rat IgG; ABclonal, AS019) diluted in 1:100 with PBS for 1 h in dark at room temperature. Fibers were carefully cut off the ovules and placed onto Poly-Prep slides (Sigma-Aldrich) after three washes with PBS and examined via confocal microscope excited at 488 nm.

To access the influence of pectins for cotton fiber development and morphology, fresh cotton ovules at 2 DPA were harvested and cultured in at 28 °C in BT medium in dark. 0.1% (w/v) of pectinase (Biotopped, P6280C) was applied into the medium. After 12h

incubation, the pectinase treated ovules were performed immunolabelling with JIM5 to test the degradation of pectins.

Assessing the thickness of cellulose in cotton fiber cell walls

The cotton ovules were harvested from fresh flowers at 10 DPA. and then fixed overnight in 4 % (w/v) paraformaldehyde in PBS buffer (pH=7) at 4 °C. Then the ovules were dehydrated in ethanol and embedded in Technovit 7100. The cotton fibers were cut into sections (thickness, 5 μm) with a Leica RM2265 microtome, and stained with 0.05 % (w/v) Calcofluor White (CFW; Sigma-Aldrich, BCCF8014) for 5 min at room temperature in dark. The stained fiber cross sections were examined under 40X objective of the ZEISS Axio observer Z1 at excitation of 445 nm. The fluorescent of CFW intensity profile was measured using Line tools of ImageJ (https://imagej.nih.gov/ij/). The FWHM was calculated through a self-written macro after the Gaussian fitting.

Scanning Electron Microscopy and S4B staining

Cotton ovules at various developmental stages (0 DPA, 3 DPA and 7 DPA) were harvested from the fresh flowers, and frozen in the liquid nitrogen via frozen transmission system (Quorum PP3010T). The samples were broken and sublimated in -70 °C for 10 min. After sputtering with platinum (10 mA, 60 s), the imaging was performed in a high-resolution SEM 7401F (JEOL, Japan).

To display the cellulose deposition by S4B staining, the ovules were collected from fresh flowers at 3 DPA and incubated with 0.1% (v/v) Tween-20 in PBS buffer (pH=7) for 5 min.

Then the samples were stained with 0.01% (w/v) S4B in PBS buffer for 15 min in dark. After three times washes, the fiber cells were cut off the ovules and placed onto slides. The fluorescent signals of stained celluloses were examined under 60X oil objective of confocal microscope with excitation at 561 nm.

CRISPR/Cas9-mediated genome editing

The CRISPR/Cas9-mediated genome editing was implied to knockout the GhCSI1 genes in both At (Gh_A11G212800) and Dt (Gh_D11G239500) of cotton genome. Dual guide RNA (sgRNA) 5'-ATCAGGATCTCTTGGAGTGA-3' and 5'-GTGCTTTGGAAGCTGCTAAA-3' was designed from both of the coding region. CRISPR-Cas9 experiments were conducted following previously reported experimental protocols [58] and performed by WIMI Biotechnology with TM-1. The edited type of GhCSI1-A and GhCSI1-D were identified via Sanger sequencing (BGI Tech Solutions Co.) to obtain homozygous gene mutants with specific primers. All the cotton lines were grown in the field under normal farming practices, or in a greenhouse with long-day (16 h light/8 h dark) conditions at 28 ℃. Mature fibers (~10 g) were collected from the bolls of similar positions (primarily the middle boll positions) to determine the fiber length parameters by Advanced Fiber Information System (AFIS).

Spinning-disc confocal microscopy and live-cell imaging

Live-cell imaging was carried out under a spinning-disk confocal microscope (Ultraview VoX, PerkinElmer, Beaconsfield, Buckinghamshire, UK) equipped with the Yokogawa Nipkow CSU-X1 spinning disk scanner, Hamamatsu EMCCD 9100-13, Nikon TiE inverted

microscopy with the Perfect Focus System. mNeoGreen was excited at 488 nm, and mCherry was excited at 561 nm. A 100X Plan Apo oil immersion TIRF objective (NA=1.49) was used for most image sequences acquisition. Each time-lapsed image stack was acquired over five minutes with 30s intervals. Acquired images were processed and analysed using Volocity (Perkin Elmer), ImageJ (http://rsbweb.nih.gov/ij), as described previously [29,59].

Computational simulation

The detailed description of cotton fiber growth model is available in Supplementary Note 1.

Quantification and statistical analysis

All statistical details (statistical test used, number of samples, and p values) for each experiment can be found in the Figure labels or legends. The statistical analyses were performed using GraphPad Prism 9 software. Data were considered statistically significant when $p < 0.05$ by statistical test performed as indicated in the Figure labels or legends. Two-tailed unpaired Student's t test was used to compare two different groups of samples when indicated.

Data availability

Source data are provided with this paper. All data generated or analyzed during this study are included in this article and its supplementary information files. Further information and requests for resources and reagents should be directed to and will be fulfilled by the lead contact, Zhaosheng Kong (zskong@im.ac.cn). All unique reagents generated in this study

are available from the lead contact upon request and with a completed material transfer agreement.

Code availability

The code used for mathematical modeling and analysis is available on Code Ocean (Capsule: “Differential Cellulose Distribution Drives Polarized Growth of Cotton Fibers”, DOI: 10.24433/CO.0498922.v1). The GitHub repository (https://github.com/zhou-biomech/DiffCMFCottonFibers) is provided as a development mirror.

References

1 Vaahtera, L., Schulz, J. & Hamann, T. Cell wall integrity maintenance during plant development and interaction with the environment. *Nat Plants* **5**, 924-932, doi:10.1038/s41477-019-0502-0 (2019).

2 Cosgrove, D. J. Structure and growth of plant cell walls. *Nat Rev Mol Cell Biol* **25**, 340-358, doi:10.1038/s41580-023-00691-y (2024).

3 Zhang, Y. *et al.* Molecular insights into the complex mechanics of plant epidermal cell walls. *Science* **372**, 706-711, doi:10.1126/science.abf2824 (2021).

4 Coen, E. & Cosgrove, D. J. The mechanics of plant morphogenesis. *Science* **379**, eade8055, doi:10.1126/science.ade8055 (2023).

5 Dehors, J. *et al.* Evolution of Cell Wall Polymers in Tip-Growing Land Plant Gametophytes: Composition, Distribution, Functional Aspects and Their Remodeling. *Front Plant Sci* **10**, 441, doi:10.3389/fpls.2019.00441 (2019).

6 Palin, R. & Geitmann, A. The role of pectin in plant morphogenesis. *Biosystems* **109**, 397-402, doi:10.1016/j.biosystems.2012.04.006 (2012).

7 Cameron, C. & Geitmann, A. Cell mechanics of pollen tube growth. *Curr Opin Genet Dev* **51**, 11-17, doi:10.1016/j.gde.2018.03.008 (2018).

8 Kim, H. J. & Triplett, B. A. Cotton fiber growth in planta and in vitro. Models for plant cell elongation and cell wall biogenesis. *Plant Physiol* **127**, 1361-1366, doi:10.1104/pp.010724 (2001).

9 Pettolino, F. A., Yulia, D., Bacic, A. & Llewellyn, D. J. Polysaccharide composition during cotton seed fibre development: temporal differences between species and in different seasons. *Journal of Cotton Research* **5**, doi:10.1186/s42397-022-00136-5 (2022).

10 Johnson, K. L. From Fuzz to Fiber: Identification of Genes Involved in Cotton Fiber Elongation. *Plant Physiology* **183**, 23-24, doi:10.1104/pp.20.00233 (2020).

11 Wen, X. *et al.* A comprehensive overview of cotton genomics, biotechnology and molecular

biological studies. *Sci China Life Sci* **66**, 2214-2256, doi:10.1007/s11427-022-2278-0 (2023).

12 Haigler, C. H., Betancur, L., Stiff, M. R. & Tuttle, J. R. Cotton fiber: a powerful single-cell model for cell wall and cellulose research. *Front Plant Sci* **3**, 104, doi:10.3389/fpls.2012.00104 (2012).

13 Qin, Y. M. & Zhu, Y. X. How cotton fibers elongate: a tale of linear cell-growth mode. *Curr Opin Plant Biol* **14**, 106-111, doi:10.1016/j.pbi.2010.09.010 (2011).

14 Yu, Y. *et al.* Live-cell imaging of the cytoskeleton in elongating cotton fibres. *Nat Plants* **5**, 498-504, doi:10.1038/s41477-019-0418-8 (2019).

15 Wang, G., Yu, Y. & Kong, Z. Visualization of Cytoskeleton Organization and Dynamics in Elongating Cotton Fibers by Live-Cell Imaging. *Methods Mol Biol* **2604**, 311-316, doi:10.1007/978-1-0716-2867-6_25 (2023).

16 Carter, R. *et al.* Stomatal Opening Involves Polar, Not Radial, Stiffening Of Guard Cells. *Curr Biol* **27**, 2974-2983 e2972, doi:10.1016/j.cub.2017.08.006 (2017).

17 Cosgrove, D. J. Diffuse Growth of Plant Cell Walls. *Plant Physiol* **176**, 16-27, doi:10.1104/pp.17.01541 (2018).

18 Peaucelle, A. *et al.* Pectin-induced changes in cell wall mechanics underlie organ initiation in Arabidopsis. *Curr Biol* **21**, 1720-1726, doi:10.1016/j.cub.2011.08.057 (2011).

19 Sampathkumar, A. *et al.* Subcellular and supracellular mechanical stress prescribes cytoskeleton behavior in Arabidopsis cotyledon pavement cells. *Elife* **3**, e01967, doi:10.7554/eLife.01967 (2014).

20 Herburger, K., Schoenaers, S., Vissenberg, K. & Mravec, J. Shank-localized cell wall growth contributes to Arabidopsis root hair elongation. *Nat Plants* **8**, 1222-1232, doi:10.1038/s41477-022-01259-y (2022).

21 Bosch, M. & Hepler, P. K. Pectin methylesterases and pectin dynamics in pollen tubes. *Plant Cell* **17**, 3219-3226, doi:10.1105/tpc.105.037473 (2005).

22 Hepler, P. K., Rounds, C. M. & Winship, L. J. Control of cell wall extensibility during pollen tube growth. *Mol Plant* **6**, 998-1017, doi:10.1093/mp/sst103 (2013).

23 Polko, J. K. & Kieber, J. J. The Regulation of Cellulose Biosynthesis in Plants. *Plant Cell* **31**, 282-296, doi:10.1105/tpc.18.00760 (2019).

24 Seagull, R. W. Cytoskeletal Involvement in Cotton Fiber Growth and Development. *Micron* (1993).

25 Vaughn, K. C. & Turley, R. B. Ultrastructural effects of cellulose biosynthesis inhibitor herbicides on developing cotton fibers. *Protoplasma* **216**, 80-93, doi:10.1007/BF02680135 (2001).

26 Li, Y. *et al.* Evolution, gene expression profiling and 3D modeling of CSLD proteins in cotton. *BMC Plant Biol* **17**, 119, doi:10.1186/s12870-017-1063-x (2017).

27 Pandey, D. K. & Chaudhary, B. Synchronous Transcription of Cytoskeleton-Associated Genes is Critical to Cotton Fiber Elongation. *Journal of Plant Growth Regulation* **38**, 1037-1061, doi:10.1007/s00344-019-09913-0 (2019).

28 Gu, Y. & Rasmussen, C. G. Cell biology of primary cell wall synthesis in plants. *Plant Cell* **34**, 103-128, doi:10.1093/plcell/koab249 (2022).

29 Schneider, R., Ehrhardt, D. W., Meyerowitz, E. M. & Sampathkumar, A. Tethering of cellulose synthase to microtubules dampens mechano-induced cytoskeletal organization in Arabidopsis pavement cells. *Nat Plants* **8**, 1064-1073, doi:10.1038/s41477-022-01218-7 (2022).

30 Li, S., Lei, L., Somerville, C. R. & Gu, Y. Cellulose synthase interactive protein 1 (CSI1) links

microtubules and cellulose synthase complexes. *Proc Natl Acad Sci U S A* **109**, 185-190, doi:10.1073/pnas.1118560109 (2012).

31 Tian, J. *et al.* Orchestration of microtubules and the actin cytoskeleton in trichome cell shape determination by a plant-unique kinesin. *Elife* **4**, doi:10.7554/eLife.09351 (2015).

32 Lei, L. *et al.* CELLULOSE SYNTHASE INTERACTIVE1 Is Required for Fast Recycling of Cellulose Synthase Complexes to the Plasma Membrane in Arabidopsis. *Plant Cell* **27**, 2926-2940, doi:10.1105/tpc.15.00442 (2015).

33 Yanagisawa, M., Keynia, S., Belteton, S., Turner, J. A. & Szymanski, D. B. A conserved cellular mechanism for cotton fibre diameter and length control. *in silico Plants* **4**, doi:10.1093/insilicoplants/diac004 (2022).

34 Paredez, A. R., Somerville, C. R. & Ehrhardt, D. W. Visualization of cellulose synthase demonstrates functional association with microtubules. *Science* **312**, 1491-1495, doi:10.1126/science.1126551 (2006).

35 Watanabe, Y. *et al.* Visualization of cellulose synthases in Arabidopsis secondary cell walls. *Science* **350**, 198-203, doi:10.1126/science.aac7446 (2015).

36 Watanabe, Y. *et al.* Cellulose synthase complexes display distinct dynamic behaviors during xylem transdifferentiation. *Proc Natl Acad Sci U S A* **115**, E6366-E6374, doi:10.1073/pnas.1802113115 (2018).

37 Sanchez-Rodriguez, C. *et al.* BRASSINOSTEROID INSENSITIVE2 negatively regulates cellulose synthesis in Arabidopsis by phosphorylating cellulose synthase 1. *Proc Natl Acad Sci U S A* **114**, 3533-3538, doi:10.1073/pnas.1615005114 (2017).

38 Du, F. & Jiao, Y. Mechanical control of plant morphogenesis: concepts and progress. *Curr Opin Plant Biol* **57**, 16-23, doi:10.1016/j.pbi.2020.05.008 (2020).

39 Wallner, E. S. *et al.* Spatially resolved proteomics of the Arabidopsis stomatal lineage identifies polarity complexes for cell divisions and stomatal pores. *Dev Cell* **59**, 1096-1109 e1095, doi:10.1016/j.devcel.2024.03.001 (2024).

40 Graham, B. P. & Haigler, C. H. Microtubules exert early, partial, and variable control of cotton fiber diameter. *Planta* **253**, 47, doi:10.1007/s00425-020-03557-1 (2021).

41 Stiff, M. R. & Haigler, C. H. Cotton fiber tips have diverse morphologies and show evidence of apical cell wall synthesis. *Sci Rep* **6**, 27883, doi:10.1038/srep27883 (2016).

42 Guerriero, G., Fugelstad, J. & Bulone, V. What do we really know about cellulose biosynthesis in higher plants? *J Integr Plant Biol* **52**, 161-175, doi:10.1111/j.1744-7909.2010.00935.x (2010).

43 Taylor, N. G. Cellulose biosynthesis and deposition in higher plants. *New Phytol* **178**, 239-252, doi:10.1111/j.1469-8137.2008.02385.x (2008).

44 Hocq, L., Pelloux, J. & Lefebvre, V. Connecting Homogalacturonan-Type Pectin Remodeling to Acid Growth. *Trends Plant Sci* **22**, 20-29, doi:10.1016/j.tplants.2016.10.009 (2017).

45 Peaucelle, A., Wightman, R. & Hofte, H. The Control of Growth Symmetry Breaking in the Arabidopsis Hypocotyl. *Curr Biol* **25**, 1746-1752, doi:10.1016/j.cub.2015.05.022 (2015).

46 Haas, K. T., Wightman, R., Meyerowitz, E. M. & Peaucelle, A. Pectin homogalacturonan nanofilament expansion drives morphogenesis in plant epidermal cells. *Science* **367**, 1003-1007, doi:10.1126/science.aaz5103 (2020).

47 Zhang, T., Tang, H., Vavylonis, D. & Cosgrove, D. J. Disentangling loosening from softening: insights into primary cell wall structure. *Plant J* **100**, 1101-1117, doi:10.1111/tpj.14519 (2019).

48 Singh, B. *et al.* A specialized outer layer of the primary cell wall joins elongating cotton fibers into tissue-like bundles. *Plant Physiol* **150**, 684-699, doi:10.1104/pp.109.135459 (2009).

49 Pang, C. Y. *et al.* Comparative proteomics indicates that biosynthesis of pectic precursors is important for cotton fiber and Arabidopsis root hair elongation. *Mol Cell Proteomics* **9**, 2019-2033, doi:10.1074/mcp.M110.000349 (2010).

50 Sun, H. *et al.* Pectate lyase-like Gene GhPEL76 regulates organ elongation in Arabidopsis and fiber elongation in cotton. *Plant Sci* **293**, 110395, doi:10.1016/j.plantsci.2019.110395 (2020).

51 Wang, H. *et al.* The essential role of GhPEL gene, encoding a pectate lyase, in cell wall loosening by depolymerization of the de-esterified pectin during fiber elongation in cotton. *Plant Mol Biol* **72**, 397-406, doi:10.1007/s11103-009-9578-7 (2010).

52 Li, W. *et al.* Genome-wide identification, phylogeny, and expression analysis of pectin methylesterases reveal their major role in cotton fiber development. *BMC Genomics* **17**, 1000, doi:10.1186/s12864-016-3365-z (2016).

53 Kelly-Bellow, R. *et al.* Brassinosteroid coordinates cell layer interactions in plants via cell wall and tissue mechanics. *Science* **380**, 1275-1281, doi:10.1126/science.adf0752 (2023).

54 Hoermayer, L. *et al.* Mechanical forces in plant tissue matrix orient cell divisions via microtubule stabilization. *Dev Cell* **59**, 1333-1344 e1334, doi:10.1016/j.devcel.2024.03.009 (2024).

55 Liu, W. *et al.* Towards a better recording of microtubule cytoskeletal spatial organization and dynamics in plant cells. *J Integr Plant Biol* **61**, 388-393, doi:10.1111/jipb.12721 (2019).

56 Wang, J. *et al.* Brassinosteroid signals cooperate with katanin-mediated microtubule severing to control stamen filament elongation. *EMBO J* **42**, e111883, doi:10.15252/embj.2022111883 (2023).

57 Zhang, T., Zheng, Y. & Cosgrove, D. J. Spatial organization of cellulose microfibrils and matrix polysaccharides in primary plant cell walls as imaged by multichannel atomic force microscopy. *Plant J* **85**, 179-192, doi:10.1111/tpj.13102 (2016).

58 Wang, P. *et al.* High efficient multisites genome editing in allotetraploid cotton (Gossypium hirsutum) using CRISPR/Cas9 system. *Plant Biotechnol J* **16**, 137-150, doi:10.1111/pbi.12755 (2018).

59 Huang, L., Zhang, W., Li, X., Staiger, C. J. & Zhang, C. Point mutations in the catalytic domain disrupt cellulose synthase (CESA6) vesicle trafficking and protein dynamics. *Plant Cell* **35**, 2654-2677, doi:10.1093/plcell/koad110 (2023).

Acknowledgments

We thank Dr. Enrico Coen (Department of Cell and Developmental Biology, John Innes Centre, UK) and Dr. Jordi Chan (Department of Cell and Developmental Biology, John Innes Centre, UK) for their insightful suggestions on plant cell wall immunolabelling. We

thank Dr. Bo Liu (Department of Plant Biology, College of Biological Sciences, University of California, Davis, CA, USA) for his valuable suggestions on live-cell imaging. We thank Dr. Jin Zhou (National Center for Nanoscience and Technology, Chinese Academy of Sciences) for helping with AFM sample scanning.

Funding statement

This study was supported by the National Key Research and Development Program of China (2022YFD1200300), the National Natural Science Foundation of China (Grant No. 31925003 and 32100556), and the fellowship of China National Postdoctoral Program for Innovative Talents (Grant No. BX20200359).

S.P. thanks the Villum Investigator (Project ID: 25915), Novo Nordisk Laureate (NNF19OC0056076), Novo Nordisk Emerging Investigator (NNF20OC0060564), and Novo Nordisk Data Science (NNF0068884) grants to S.P.

Author contributions

Z.K. and G.W. designed the project. G.W., J.W. and H.Y. performed most of the experiments. J-X.W. generated the figures in the manuscript. Y.Y., X.Z. and J.T. helped with most of sample and reagent preparation. Y.M. helped with the plant material preparation. L.Z helped with the computational modeling. G.X., Y.X. and S.P. helped with writing of the manuscript. L.Z. and Z.K. supervised the project.

Competing interests

The authors declare no competing interests.

Figure legends

Fig. 1 | Mechanical features of cotton fiber primary cell walls reflect a tip-biased diffused growth mode.
a, SEM images showing the fiber cells initiated from cotton ovule (0DPA) and followed by a rapid elongation stages (3 DPA and 7 DPA). Scale bars indicate 50 μm. The experiment was repeated independently three times with similar results. **b,** AFM maps of modulus show the mechanical features of cotton fiber cell walls between different cotton cultivars (*G. hirsutum* cv. TM-1 and *G. barbadense* cv. Hai7124) at 3 and 7 DPA. Warmer colors indicate higher modulus. Scale bars indicate 100 nm. **c**, Comparison of cell wall mechanical parameters, the modulus and stiffness, at fiber apex regions for TM-1 (*G. hirsutum*) and Hai7124 (*G. barbadense*) at 3 and 7 DPA. Colors distinguish cultivars. Box plots show the median and interquartile range, whiskers indicate the minimum and maximum values. n = 9 fibers from three different ovules were considered for each group. Statistically significant differences between groups were tested using two-way ANOVA with post-hoc Sidak's test for multiple comparison. **d,** Comparison of cell wall mechanical parameters, the modulus and stiffness, at different positions of TM-1 fibers at 3 and 7 DPA. Colors distinguish developmental stages. Error bars indicate SD. n = 9 fibers from three different ovules were considered for each group. Statistically significant differences between groups were tested using two-way ANOVA with post-hoc Sidak's test for multiple comparison. Exact P values are shown in the figure panels. **e,** Osmotic deformation analysis for 3 DPA fibers before (water) and after hyperosmotic (0.8 M mannitol) conditions. Images were acquired from the same ovule region before and after medium exchange; due to dense fiber packing, individual-fiber pairing could not be reliably ensured. Arrows indicate the locations where fiber width was measured. Scale bars indicate 20 μm. **f,** Comparisons of fiber width between water and hyperosmotic treatment at the tip and shanks as indicated in **e**. Box plots show the median and interquartile range, whiskers indicate the minimum and maximum values. n = 40 fibers from four ovules were considered. Statistically significant differences between groups were tested using one-way ANOVA with post-hoc Sidak's test for multiple comparison. Exact p-values were indicated in the panels.

Fig. 2 | Visualization of cell wall synthesis in fiber cells with the click-chemistry-based method.
a, Clickable reaction to generated Cy5-labeled cellulose in cell walls. **b**, Cartoon schematic showing the chase labeling of newly synthesized cell walls of fiber cells via feeding azido-glucose (aGlu) to cultured ovules at different periods. After conjunction with DBCO-Cy5, the newly formed cell walls could be observed under confocal microscopy. **c**,

Confocal images showing the Cy5-labeled cell walls of fiber cells (3DPA) after a four-hour absorption of aGlu. Yellow or black circles highlight the newly formed cell walls at the tip regions of fiber cells. Scale bars, 10 μm. The experiment was repeated independently over three times with similar results.

Fig. 3 | A cellulose accumulation gradient supports directed cotton fiber elongation. **a,** Evaluation of the thickness of cellulose (stained by CFW, left panel) in the tip (top panels) and the shank (bottom panels) in cotton fiber cell walls (10 DPA). The intensity of CFW signals (blue dotted lines, right panels) are fitted by gaussian distributions (red shadows, right panels). The red double head arrows (right panels) indicate the FWHW of CFW fluorescent intensity that represents the thickness of celluloses in fiber cell walls. Scale bars, 10 μm. **b,** Comparison of cellulose thickness between the tip and shank region of cotton fiber cell walls. Box plots show the median and interquartile range, whiskers indicate the minimum and maximum values. n = 11 fiber cells from four ovules of each group were taken into account. Statistically significant differences between groups were tested using a two-sided unpaired *t* test. Exact P values are shown in the figure panels. **c,** S4B staining shows the differential accumulation of cellulose microfibrils between tip and shank region of cotton fiber cell walls (3 DPA), scale bar, 5 μm. **d,** The shank regions of cotton fiber cell walls exhibit higher content of cellulose microfibrils deposition as suggested by S4B fluorescent intensity. Box plots show the median and interquartile range, whiskers indicate the minimum and maximum values. n = 11 fibers from four ovules were taken into account. Statistically significant differences between groups were tested using a two-sided unpaired *t* test. Exact P values are shown in the figure panels. **e,** Cross sections of cotton fibers (10 DPA) at the tip region were stained with CFW showing the cellulose-rich wall ring (left, scale bar, 10 μm). The CFW-labelled wall thickness (indicated by CFW FWHW intensity) was proportional to the diameters of cotton fiber cross sections (right, n=12). The red fitted line indicates linear regression.

Fig. 4 | Distribution and dynamic behavior of CSCs in cotton fiber cells.
a, Live-cell imaging shows the distribution of CSCs and organization of microtubules in growing cotton fiber cells (2 DPA). The mNeoGreen-GhCESA3 foci (green) accumulate on the plasma membrane and exhibit linear trajectories distribution (yellow dotted lines) that is co-localized with microtubules (magenta). Yellow arrows indicated SmaCCs. Scale bars, 5 μm. The experiment was repeated independently over five times with similar results. **b,** Confocal images show the distribution of CESA3 foci in fiber cells at initiation (left, 0 DPA) and elongation stages (right, 2 DPA). Scale bars, 10 μm. The experiment was repeated independently over five times with similar results. **c,** Time-lapsed images (top panels) show the motility of CESA3 foci. Yellow and cyan circles indicate two individual CESA3 foci, and the yellow dotted line represents a base line. The cyan arrows

highlight the region and direction used for the kymograph analyses (bottom panels). **d,** Motility of CESA3 foci in different types of cells. Box plots show the median and interquartile range, whiskers indicate the minimum and maximum values. n = 11 fibers from four ovules of each group were taken into account. More than 200 events of each group were identified. Statistically significant differences between groups were tested using one-way ANOVA with post-hoc Tukey test for multiple comparison. Numbers represent detailed P values. **e**, Confocal images showing the differential distribution of CESA3 foci between cotton fiber tips and shanks. Scale bars, 10 μm. **f** and **g,** Comparison of CESA3 foci motility **f** and density **g** in different regions of cotton fibers at the elongation stage. Box plots show the median and interquartile range, whiskers indicate the minimum and maximum values. n = 11 fibers from four ovules of each group were taken into account. More than 200 events were identified. Statistically significant differences between groups were tested using two-sided unpaired *t* test or one-way ANOVA with post-hoc Tukey test for multiple comparison. Exact P values are shown in the figure panels.

Fig. 5 | Differential CMF deposition mediated by microtubules affects cotton fiber elongation.

a, 3D reconstruction confocal images show the microtubule organization in fiber cells at initiation (0 DPA) and elongation stages (2 DPA). Yellow arrow indicates MDZ in elongating fiber cells, and yellow asterisks indicate microtubules in apex of fiber cells at initiation stage. The yellow bracket indicates tip region of cotton fiber cell. Spacing between adjacent grid crosses on the sphere corresponds to 22 μm. **b** and **c,** Representative confocal images (Scale bars, 10 μm) of microtubule organization in tip and shank regions of growing cotton fiber cells (2 DPA) **b** show increased microtubule density at the shank regions **c**. Box plots show the median and interquartile range, whiskers indicate the minimum and maximum values. 11 fibers from four ovules were taken into account. Statistically significant differences between groups were tested using a two-sided unpaired *t* test. Exact P values are shown in the figure panels. **d** and **e,** Confocal images of microtubule organization in cultured fiber cells after drug treatment. Scale bars, 10 μm **d**. Either propyzamide or Taxol treatment could narrow the microtubule density between tip and shanks of cotton fiber cells **e**. Box plots show the median and interquartile range, whiskers indicate the minimum and maximum values. n = 9 fibers from three ovules of each group were taken into account. Statistically significant differences between different fiber regions and drug treatment were tested using ANOVA with post-hoc Tukey test for multiple comparison. Exact P values are shown in the figure panels. **f** Chase labeling of newly formed cell walls in fiber cells after drug treatment. Dashed circles and yellow arrows highlight the newly formed cell walls. Scale bars, 5 μm. The experiment was repeated independently over three times with similar results. **g,** Representative simulation result showing strains of each region of the cell walls (red boxes) along the model with differentially deposited CMFs. For the sake of visual

presentation, only 1/50 of the CMF-associated springs in amounts are drawn in the figure. **h,** Quantification of deformation strains along the cell walls. Ten rounds of simulations were applied under three different conditions. Error bars indicate SD. **i,** Proposed model of differentially deposited CMFs mediated by microtubules could transfer unidirectional turgor pressure into growing driven force, and exhibit a tip-biased diffuse growth mode.

Editorial summary:
Here the authors show that microtubules guide the spatial distribution of cellulose synthase complexes in cotton fibers and produce a gradient of cellulose microfibrils that creates patterned cell wall mechanics that support tip-biased elongation.

Peer review information: *Nature Communications* thanks Notburga Gierlinger, and the other, anonymous, reviewer(s) for their contribution to the peer review of this work. A peer review file is available.

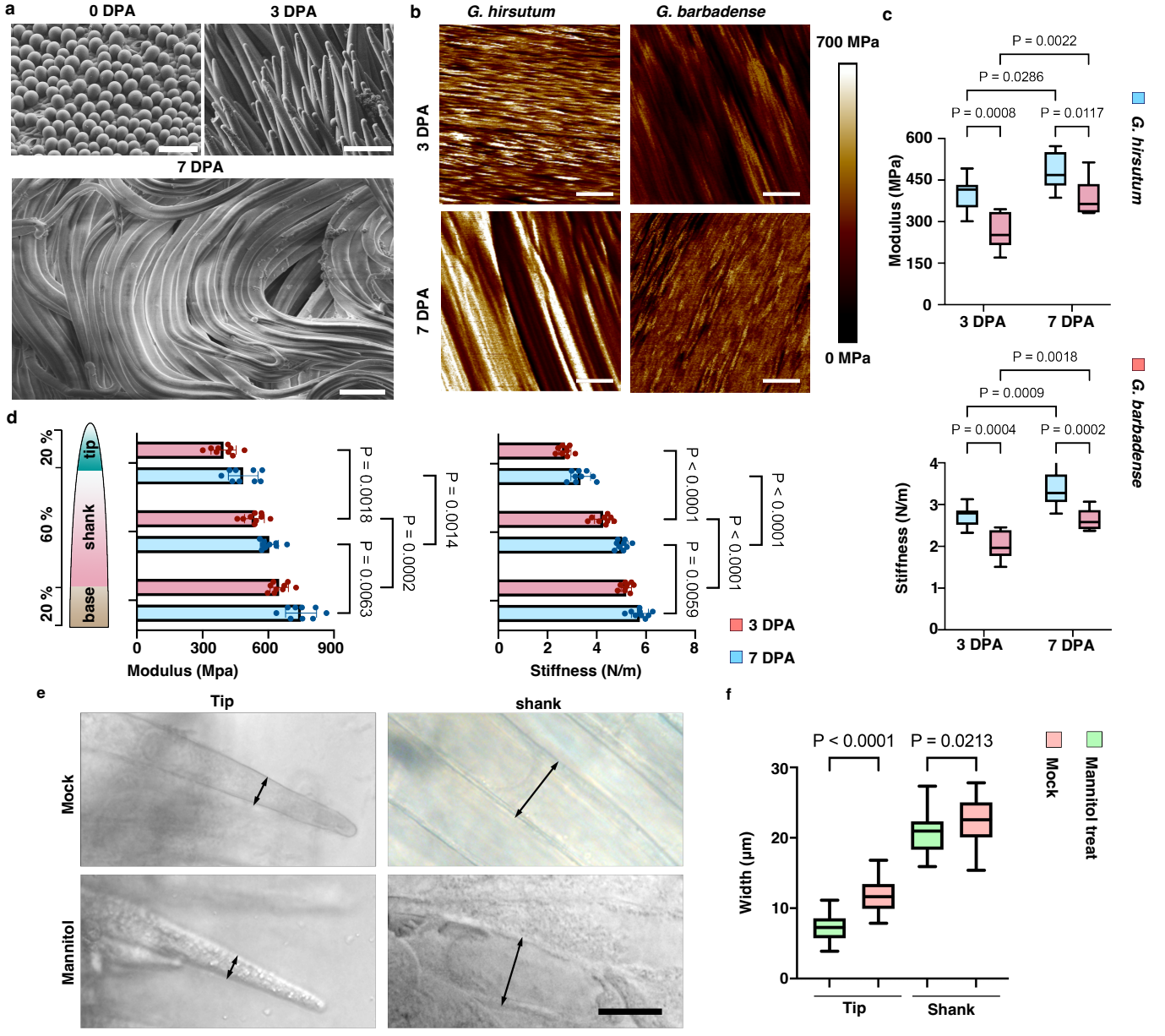
a
0 DPA
3 DPA
7 DPA
b
G. hirsutum
G. barbadense
3 DPA
7 DPA
700 MPa
0 MPa
c
P = 0.0022
P = 0.0286
P = 0.0008
P = 0.0117
Modulus (MPa)
600
450
300
150
0
3 DPA
7 DPA
G. hirsutum
P = 0.0018
P = 0.0009
P = 0.0004
P = 0.0002
Stiffness (N/m)
4
3
2
1
0
3 DPA
7 DPA
G. barbadense
d
20 %
60 %
20 %
tip
shank
base
P = 0.0018
P = 0.0014
P = 0.0063
P = 0.0002
0
300
600
900
Modulus (Mpa)
P < 0.0001
P < 0.0001
P = 0.0059
P < 0.0001
0
2
4
6
8
Stiffness (N/m)
3 DPA
7 DPA
e
Tip
shank
Mock
Mannitol
f
P < 0.0001
P = 0.0213
Width (µm)
30
20
10
0
Tip
Shank
Mock
Mannitol treat

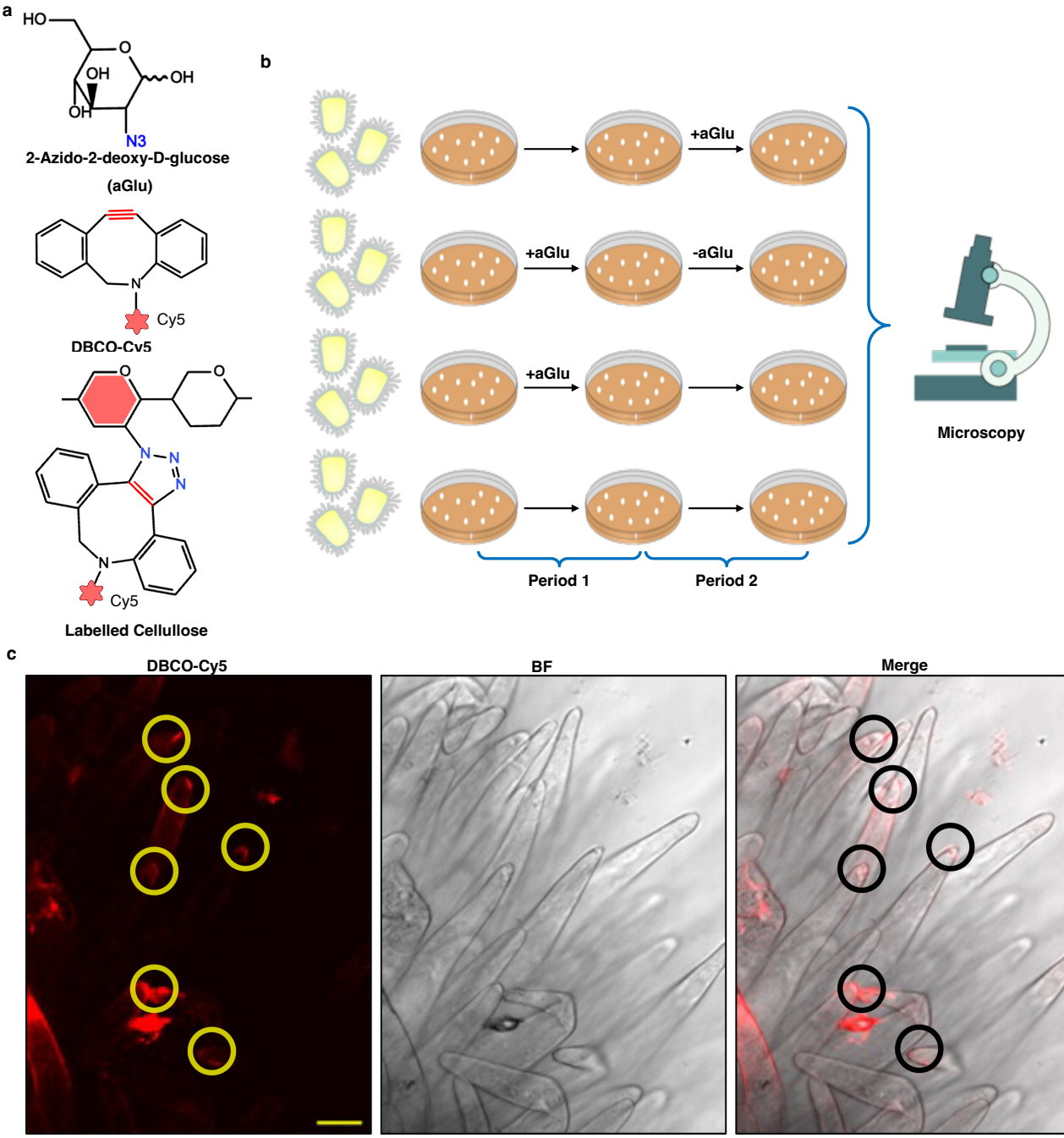
a
HO
O
OH
OH
OH
N3
2-Azido-2-deoxy-D-glucose
(aGlu)
N
Cy5
DBCO-Cy5
O
O
N
N
N
N
Cy5
Labelled Cellullose
b
+aGlu
+aGlu
-aGlu
+aGlu
Period 1
Period 2
Microscopy
c
DBCO-Cy5
BF
Merge

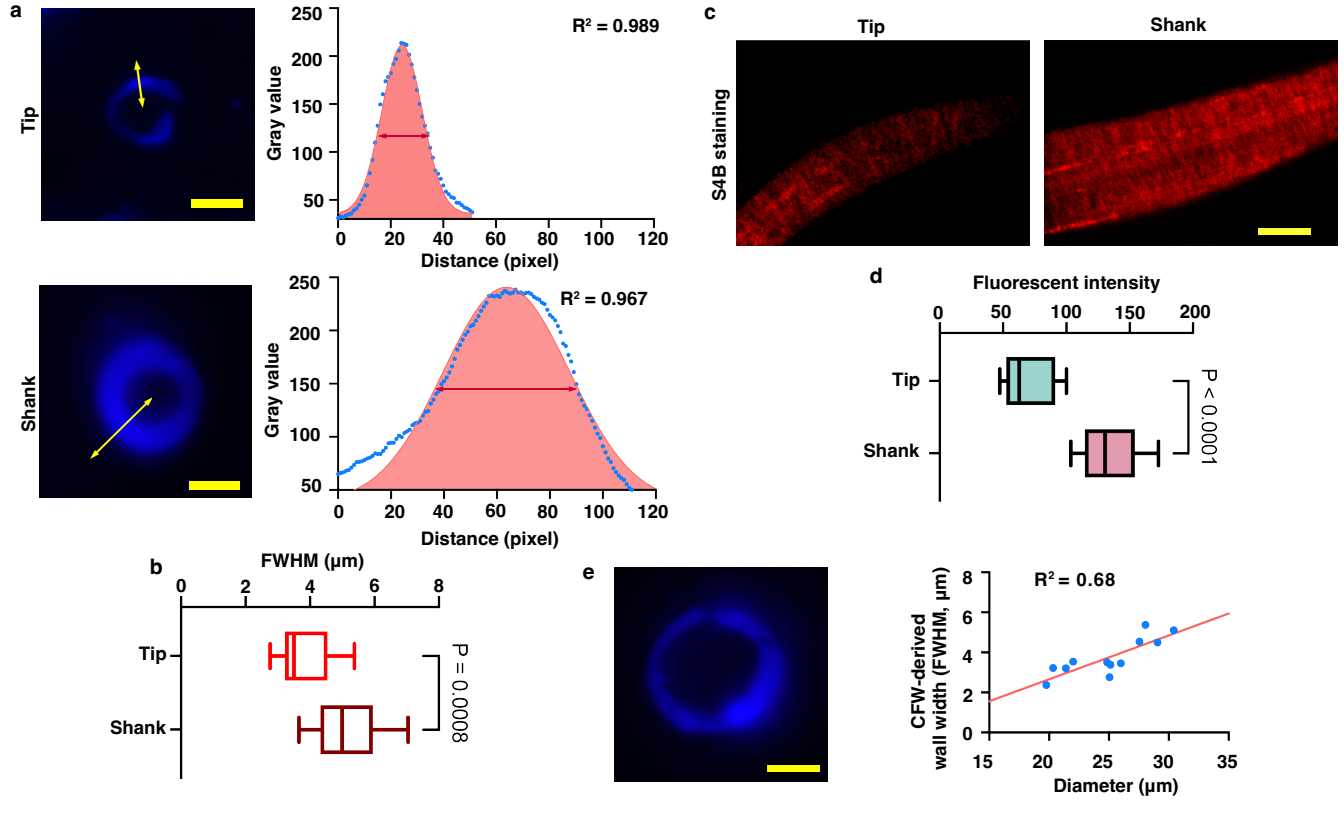
a
Tip
Shank
Gray value
Distance (pixel)
R² = 0.989
R² = 0.967
c
Tip
Shank
S4B staining
d
Fluorescent intensity
Tip
Shank
P < 0.0001
b
FWHM (μm)
Tip
Shank
P = 0.0008
e
CFW-derived wall width (FWHM, μm)
Diameter (μm)
R² = 0.68

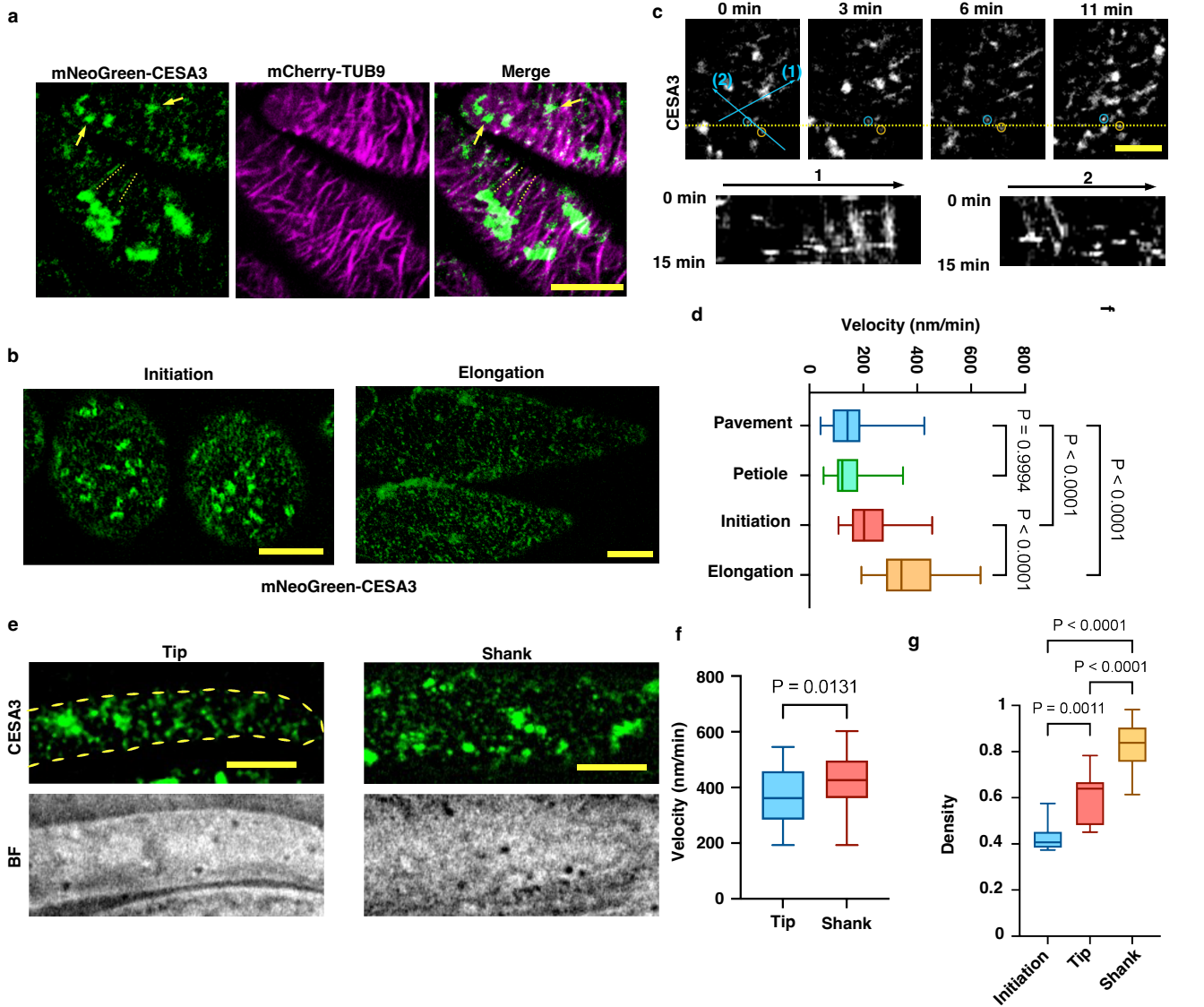
a
mNeoGreen-CESA3
mCherry-TUB9
Merge
b
Initiation
Elongation
mNeoGreen-CESA3
c
0 min
3 min
6 min
11 min
CESA3
(2)
(1)
1
2
0 min
15 min
0 min
15 min
d
Velocity (nm/min)
0
200
400
600
800
Pavement
Petiole
Initiation
Elongation
P = 0.9994
P < 0.0001
P < 0.0001
P < 0.0001
e
Tip
Shank
CESA3
BF
f
P = 0.0131
Velocity (nm/min)
800
600
400
200
0
Tip
Shank
g
P < 0.0001
P < 0.0001
P = 0.0011
Density
1
0.8
0.6
0.4
0.2
0
Initiation
Tip
Shank

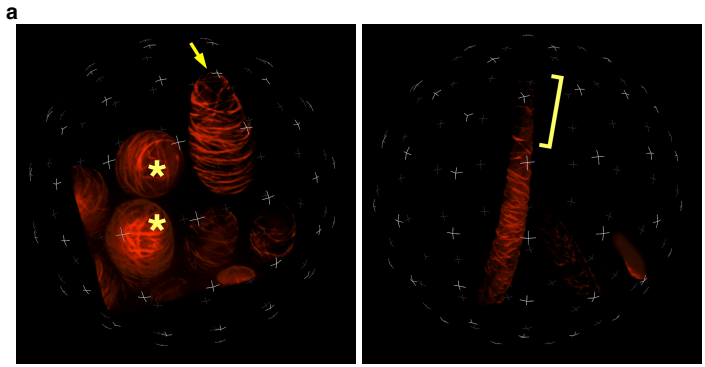
a

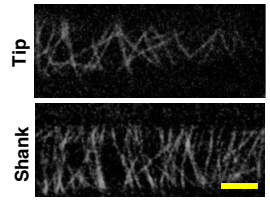
b
Tip
Shank

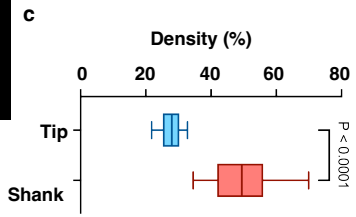
c
Density (%)
0
20
40
60
80
Tip
Shank
P < 0.0001

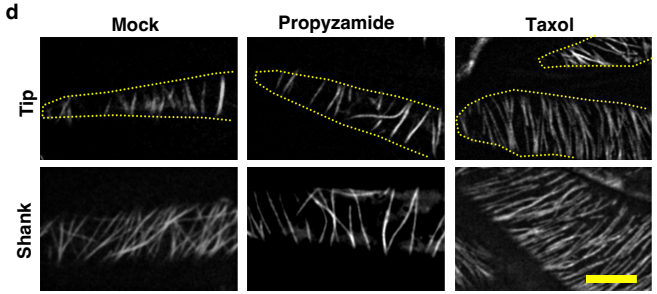
d
Mock
Propyzamide
Taxol
Tip
Shank

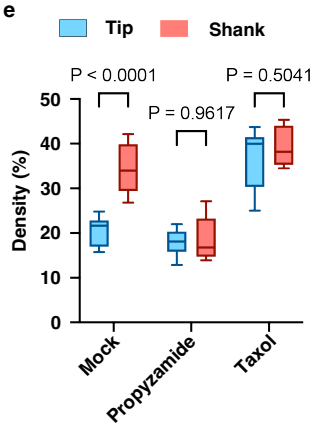
e
Tip
Shank
P < 0.0001
P = 0.9617
P = 0.5041
Density (%)
50
40
30
20
10
0
Mock
Propyzamide
Taxol

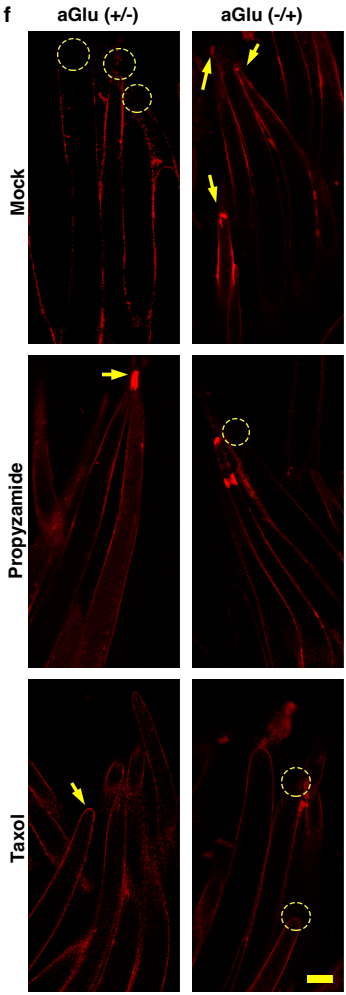
f
aGlu (+/-)
aGlu (-/+)
Mock
Propyzamide
Taxol

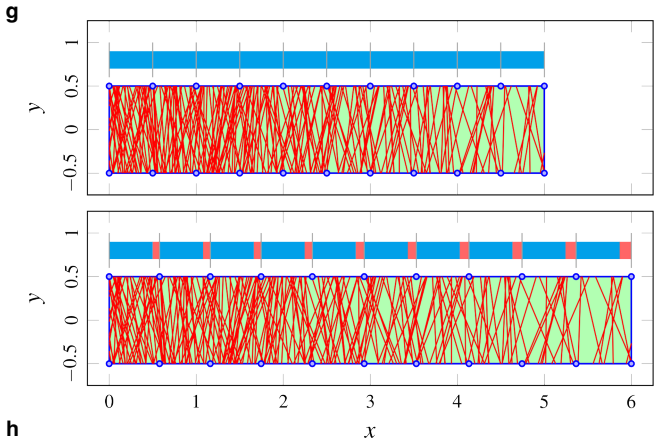
g
y
1
0.5
0
−0.5
0
1
2
3
4
5
6
x

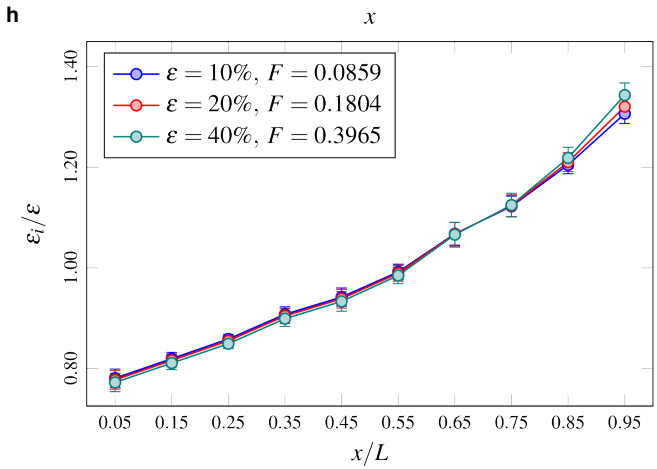
h
ε = 10%, F = 0.0859
ε = 20%, F = 0.1804
ε = 40%, F = 0.3965
εi/ε
1.40
1.20
1.00
0.80
0.05
0.15
0.25
0.35
0.45
0.55
0.65
0.75
0.85
0.95
x/L

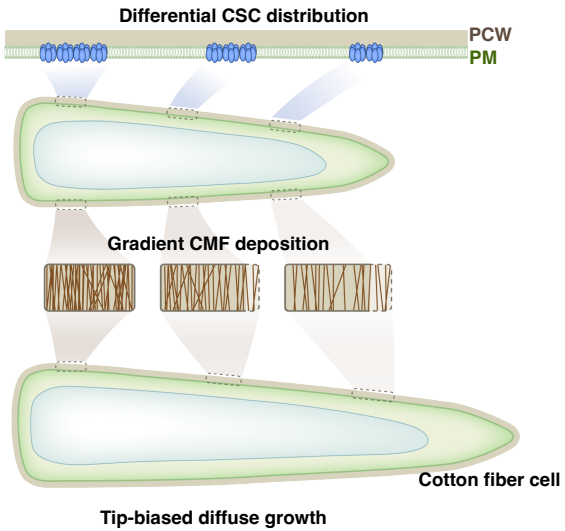
i
Differential CSC distribution
PCW
PM
Gradient CMF deposition
Cotton fiber cell
Tip-biased diffuse growth